IET Generation, Transmission & Distribution

Research Article

Fault location based on travelling wave identification using an adaptive extended Kalman filter

ISSN 1751-8687
Received on 11th June 2017
Revised 12th September 2017
Accepted on 18th October 2017
E-First on 9th February 2018
doi: 10.1049/iet-gtd.2017.0897
www.ietdl.org

Yanhui Xi[1] ✉, Zewen Li[1], Xiangjun Zeng[1], Xin Tang[1], Xiaodong Zhang[1], Hui Xiao[1]

[1]Hunan Province Higher Education Key Laboratory of Power System Safety Operation and Control, Changsha University of Science and Technology, Changsha 410114, Hunan Province, People's Republic of China

✉ *E-mail: xiyanhui@126.com*

Abstract: The fault location in transmission systems remains a challenging problem, primarily due to the fault location near the substation ends or the weak fault signals. In this study, an adaptive extended Kalman filter (EKF) based on the maximum likelihood (ML) is proposed to estimate the instantaneous amplitudes of the travelling waves. In this method, the EKF algorithm is used to estimate the optimal states (the clean travelling waves) with additive white noise while ML is used to adaptively optimise the error covariance matrices and the initial conditions of the EKF algorithm. Using the proposed method, the singularity points of travelling waves can be detected, and the exact arrival time of the initial wave head at the substations M and N can be easily yielded. Thus the fault distance can be calculated precisely. The effectiveness of exacting mutation feature using the proposed method has been demonstrated by a simulated instantaneous pulse. Also, the proposed method has been tested with different types of faults, such as different fault locations, different fault resistances and different fault inception angles using ATP simulation. The accuracy of fault location using the proposed method has been compared with conventional wavelet transformation scheme.

1 Introduction

Travelling wave-based fault location is the most important scheme used to accurately pinpoint faults on transmission lines. It has the advantage of high accuracy, immunity to power swings, and insensitivity to various fault conditions such as fault type, fault inception angle and fault resistance. Therefore, it attracts the increasing interests of researchers and engineers within the field [1–4].

As travelling wave-based fault location methods, single-ended fault location method and double-ended method are the main methods. Compared with single-ended fault location method, the double-ended method is usually more reliable and more accurate because it merely needs the initial surge but not the subsequence travelling waves. Furthermore, the double-ended travelling wave method has the potential to locate many forms of disturbances besides the usual lightning strike occurrence.

For the double-ended travelling wave method, the key factor is to determine the exact arrival time of the initial travelling wave. Transient travelling wave signal has an obvious singularity after the fault occurred. Wavelet transform (WT), as an analysis tool for signals in time-domain and frequency-domain, can detect the transient signal singularity effectively, which is suitable for identifying transient travelling waves. In [5], wavelet analysis is presented to provide time resolution for high resistive zero-crossing fault detection based on transient signals. Likewise, discrete wavelet transformation is applied to the DC voltage and current signals in segmented HVDC transmission line in [6]. In [7], a general method based on phase-mode transformation and wavelet transformation is proposed for fault-location in the complex power grid. Although the WT method shows good results in determining the fault type and location, it exhibits some disadvantages, such as complicated computation, sensitivity to the noise level, and the dependency of its accuracy on the selection of mother wavelet. The most important limitation of the existing methods based on the wavelet transformation is not time shift invariant, which means that there is no correlation between the original signal and WT coefficients. Recently, some hybrid techniques using combined wavelet, support vector machines [8, 9], artificial neural network [10–12] and fuzzy logic [13] have been applied for travelling wave-based fault location of transmission lines. Although these combinations may perform better than the single WT, they have more computational complexity. Moreover, they still suffer from the limitations of the WT.

On the other hand, Hilbert–Huang transform (HHT), which is considered the most adaptive technique for analysing the non-linear and non-stationary signals, is developed to analyse power system fault signal and has a better effect in fault location (see, e.g. [14–18]). HHT is composed of empirical mode decomposition (EMD) and the Hilbert transform (HT). The fault (travelling wave) signal is firstly decomposed into intrinsic mode function (IMF) by the EMD method. Then instantaneous frequency and instantaneous amplitude are obtained by HT to compose Hilbert spectrum. Thus the transient caused by fault can be analysed and further detected accurately through the instantaneous frequency and the time–frequency–amplitude spectra analysis. HHT can overcome the shortcomings of WT and has been proved to be one of the best methods for instantaneous frequency feature extraction in power fault detection applications. However, EMD as the main step in HHT still has defects, such as the overshoot or undershoot phenomenon in theory. A different stopping condition for the EMD calculation loop may produce a different set of IMFs, and the resulting IMF may not accurately reflect the true physical nature of the analysed data because the EMD tends to miss some riding waves on the steep edge of the IMF. At the same time, HT may result in a negative frequency at times, which is extremely hard to interpret and is of debatable physical significance.

Although the aforementioned algorithms are reliable, they may suffer from inaccuracies in some cases. First, in order to determine the arrival time of the wave head, it often requires a higher sampling rate of the protective device. However, the high sampling rate is easy to be interfered by all kinds of noises. Besides, the travelling wave signal itself contains a lot of noise because travelling wave recorders are usually set with a low threshold to capture as many fault travelling waves as possible for an event analysis, which reduces the chance of missing true fault events, but also increases the amount of unwanted noise-triggered data to be recorded. Second, travelling wave signals, which are generated by a single phase-to-ground fault with 0° inception angle or high fault resistances, may be very weak, and the indistinct wave front will be

© The Institution of Engineering and Technology 2017

hardly identified for the detection purpose. Therefore, to improve the reliability of travelling wave detection, as well as maintains the capability of fast fault detection, it is necessary to explore the effective double-ended travelling wave data identification and correlation matching method.

To extract the wave head of the travelling wave signal, some digital filtering approaches based on time-domain, such as the least error square method and the least square method, have been developed to determine the fault type and location. However, most of these algorithms have several limitations in terms of inaccuracies due to the presence of noise. On the contrary, the Kalman filtering (KF) method is completely based on time-domain, instead of converting the signal to the frequency domain space, so there is no problem of phase shift or amplitude attenuation in the KF. It has been proved to be one of the best methods for estimating amplitude, phase, and frequency of the fundamental and harmonic components of a signal disturbed by white noise in power quality problem [19–21]. However, still few literature have been found in power fault detection applications.

In this paper, a more robust and adaptive extended Kalman filter (EKF) algorithm based on maximum likelihood (ML) is proposed to analyse travelling wave signals and to determine the fault location. In the proposed EKF-ML method, the ML method is used to adaptively optimise the error covariance matrices $\boldsymbol{R}$, $\boldsymbol{Q}$ and the initial conditions, and the EKF is used to estimate the amplitude (states) and can directly extract the signal of the wave head, not need to filter collected waveform. In this way, the damage of the wave head information in the filtering process can be avoided. Hence, the EKF-ML algorithm makes the observed results the most probable given the model and can obtain better performance relative to the conventional EKF (the conventional EKF assumed parameter values of the error covariance matrices as specified values). Another advantage of this algorithm is that it almost has the same computational complexity as the conventional EKF. Thus, the EKF-ML algorithm is simpler and less complex than other adaptive algorithms, such as the adaptive unscented Kalman filter algorithm [22], adaptive particle swarm optimisation (APSO) of unscented Kalman filter [23, 24], the unscented Kalman smoother algorithm [25] and genetic algorithm APSO aided unscented Kalman filter [26]. All in all, the EKF-ML algorithm can quickly and accurately detect the wave head for fault location without damaging the wave head in the time domain at different fault locations, different fault inception angles, and different fault resistances. Also, the proposed adaptive EKF algorithm is capable of accurately estimating the noise parameters and is robust against various noise levels.

The main contribution of this paper is twofold. First, the use of the ML method to adaptively optimise the error covariance matrices $\boldsymbol{R}$, $\boldsymbol{Q}$ and the initial conditions, which can make sure that the EKF has better accuracy and faster convergence. Second, the proposed EKF-ML algorithm is applied to the fault location based on travelling wave.

The remaining of this paper is organised as follows. In Section 2, we propose the state-space model of the power signal. Section 3 describes the EKF-ML method. Section 4 presents simulation studies of the EKF-ML and the WT. Some concluding remarks are contained in Section 5.

2 State-space model of the travelling wave

The transient travelling wave initiated by faults is considered as a kind of abrupt signal, theoretically which is the linear combination of fundamental component, some harmonic components and all kinds of noise in steady state and a sharp rise in a very short time. Therefore, the observed transient travelling wave signal can be expressed as

$$y_k = A_{1,k}\cos(\omega k T_{\mathrm{s}} + \varphi_1) + \sum_{r=2}^{M} A_{r,k}\cos(r\omega k T_{\mathrm{s}} + \varphi_r) + u_k + v_k \quad (1)$$

where y_k (k represents the sampling point number) is the observed transient travelling wave signal, and $A_{1,k}$, ω φ_1 denote the amplitude, angular frequency, and initial phase angle of the fundamental component, respectively, and $A_{r,k}(r = 2, \ldots, M)$, φ_r denote the amplitude and initial phase angle of the rth harmonic component, respectively. u_k is the travelling wave head, which is very similar to the mutation characteristic of the pulse signal. v_k represents a zero-mean white noise with unknown covariance $E(v_k v_k^{\mathrm{T}}) = R_k$. M is the highest order of the harmonic component, and T_{s} is the sampling interval, which can be obtained as $1/f_{\mathrm{s}}$ (f_{s} is the sampling frequency).

The travelling wave head can be distinguished through detecting the variation of the travelling wave amplitude using the EKF. Thus, unknown states variables $\boldsymbol{X}_k = [x_{1,k}, x_{2,k}, \ldots, x_{2r-1,k}, x_{2r,k}, \ldots, x_{2M-1,k}, x_{2M,k}]^{\mathrm{T}}$ are assumed (see (2)) . By considering state variables above, model (1) can be rewritten in the form of state space as follows:

$$\begin{cases} \boldsymbol{X}_k = \boldsymbol{F}\boldsymbol{X}_{k-1} + \boldsymbol{\eta}_k \\ \quad = \begin{bmatrix} \boldsymbol{F}_1 & 0 & \cdots & 0 & 0 \\ 0 & \ddots & 0 & \cdots & 0 \\ 0 & \cdots & \boldsymbol{F}_r & 0 & 0 \\ 0 & \cdots & 0 & \ddots & 0 \\ 0 & \cdots & \cdots & 0 & \boldsymbol{F}_M \end{bmatrix} \begin{bmatrix} x_{1,k-1} \\ x_{2,k-1} \\ \vdots \\ x_{2r-1,k-1} \\ x_{2r,k-1} \\ \vdots \\ x_{2M-1,k-1} \\ x_{2M,k-1} \end{bmatrix} + \boldsymbol{\eta}_k \quad \boldsymbol{\eta}_k \sim N(0, \boldsymbol{Q}_k) \\ y_k = \boldsymbol{H}\boldsymbol{X}_k + \boldsymbol{v}_k \quad \boldsymbol{v}_k \sim N(0, \boldsymbol{R}_k) \end{cases} \quad (3)$$

Here, $\boldsymbol{F}$, $\boldsymbol{H}$ denote the system matrix and the observation matrix, respectively. $\boldsymbol{\eta}_k$ and $\boldsymbol{v}_k$ are the process noise and the observation noise, which are zero-mean Gaussian random variables with covariance $\boldsymbol{Q}_k$ and $\boldsymbol{R}_k$, respectively. And the matrices $\boldsymbol{F}_r$, $\boldsymbol{H}$, $\boldsymbol{Q}_k$, $\boldsymbol{R}_k$ are defined as

$$\begin{cases} \boldsymbol{F}_r = \begin{bmatrix} \cos(r\omega T_{\mathrm{s}}) & -\sin(r\omega T_{\mathrm{s}}) \\ \sin(r\omega T_{\mathrm{s}}) & \cos(r\omega T_{\mathrm{s}}) \end{bmatrix} \quad (r = 1, \ldots, M) \\ \boldsymbol{H} = [1 \quad 0 \quad \cdots \quad 1 \quad 0 \quad \cdots \quad 1 \quad 0] \\ \boldsymbol{Q}_k = \mathrm{diag}\left(\left[\gamma_1^2, \gamma_2^2, \ldots, \gamma_{2r-1}^2, \gamma_{2r}^2, \ldots, \gamma_{2M-1}^2, \gamma_{2M}^2\right]\right) \\ \boldsymbol{R}_k = \left[\varepsilon^2\right] \end{cases} \quad (4)$$

In (4), all the unknown constant parameters $(\gamma_1, \gamma_2, \ldots, \gamma_{2M-1}, \gamma_{2M}, \varepsilon))$ should be optimised. Thus, the amplitude of each frequency component can be calculated as

$$A_{r,k} = \sqrt{(x_{2r-1,k})^2 + (x_{2r,k})^2} \quad (5)$$

where $x_{2r-1,k}$ $x_{2r,k}$ can be obtained as estimated states from the model (3).

$$\begin{aligned} x_{1,k} &= A_{1,k}\cos(\omega k T_{\mathrm{s}} + \varphi_1), & x_{2,k} &= A_{1,k}\sin(\omega k T_{\mathrm{s}} + \varphi_1) \\ &\vdots \\ x_{2r-1,k} &= A_{r,k}\cos(r\omega k T_{\mathrm{s}} + \varphi_r), & x_{2r,k} &= A_{r,k}\sin(r\omega k T_{\mathrm{s}} + \varphi_r) \\ &\vdots \\ x_{2M-1,k} &= A_{M,k}\cos(M\omega k T_{\mathrm{s}} + \varphi_M), & x_{2M,k} &= A_{M,k}\sin(M\omega k T_{\mathrm{s}} + \varphi_M) \end{aligned} \quad (2)$$

© The Institution of Engineering and Technology 2017

3 EKF-ML method

The purpose here is to determine all the unknown constant parameters and to estimate the state $\boldsymbol{X}_k$ from the noisy observations using model (3). This is a type of non-linear filtering problem, for which we use the EKF to estimate the state from the noisy observations. However, the practical application of the EKF has been limited by the difficulties in selecting the process noise parameter $\boldsymbol{Q}_k$ and the observation noise parameter $\boldsymbol{R}_k$, which affects seriously the rate of convergence and the estimation performance. Thus, to obtain the best estimation, it is proposed in this paper to use the ML method for the optimal choice of the noise covariance matrices$\boldsymbol{Q}_k$ and $\boldsymbol{R}_k$.

3.1 State estimation by the EKF

Let $\hat{\boldsymbol{X}}_{k|k-1}$, $\boldsymbol{S}_{k|k-1}$ denote the conditional mean and conditional covariance of $\boldsymbol{X}_k$ given $y_{1:k-1} = \{y_1, \ldots, y_{k-1}\}$, $\hat{v}_k$ be the predicted innovation of y_k. Therefore, the prediction equations using the recursive EKF may be given as follows:

$$\begin{cases} \hat{\boldsymbol{X}}_{k|k-1} = E\{\boldsymbol{X}_k | y_{1:k-1}\} = \boldsymbol{F}\hat{\boldsymbol{X}}_{k-1|k-1} \\ \hat{v}_k = y_k - \boldsymbol{H}\hat{\boldsymbol{X}}_{k|k-1} \\ \boldsymbol{S}_{k|k-1} = E\left\{\left(\boldsymbol{X}_k - \hat{\boldsymbol{X}}_{k|k-1}\right)\left(\boldsymbol{X}_k - \hat{\boldsymbol{X}}_{k|k-1}\right)^{\mathrm{T}}\right\} = \boldsymbol{F}\boldsymbol{S}_{k-1|k-1}\boldsymbol{F}^{\mathrm{T}} + \boldsymbol{Q}_k \end{cases} \tag{6}$$

Let $\hat{\boldsymbol{X}}_{k|k}$, $\boldsymbol{S}_{k|k}$ denote the conditional mean and conditional covariance of $\boldsymbol{X}_k$ given $y_{1:k} = \{y_1, \ldots, y_k\}$, $\hat{\Psi}_k$ be the covariance of v_k, then the filtered state is given as

$$\begin{cases} \hat{\boldsymbol{X}}_{k|k} = \mathrm{E}\{\boldsymbol{X}_k | y_{1:k}\} = \hat{\boldsymbol{X}}_{k|k-1} + \boldsymbol{K}_k\hat{v}_k \\ \boldsymbol{S}_{k|k} = \mathrm{E}\left\{(\boldsymbol{X}_k - \hat{\boldsymbol{X}}_{k|k})(\boldsymbol{X}_k - \hat{\boldsymbol{X}}_{k|k})^{\mathrm{T}}\right\} = [\boldsymbol{I} - \boldsymbol{K}_k\boldsymbol{H}]\boldsymbol{S}_{k|k-1} \\ \hat{\Psi}_k = \mathrm{E}\left\{\hat{v}_k\hat{v}_k^{\mathrm{T}}\right\} = \boldsymbol{H}\boldsymbol{S}_{k|k-1}\boldsymbol{H}^{\mathrm{T}} + \boldsymbol{R}_k \\ \boldsymbol{K}_k = \boldsymbol{S}_{k|k-1}\boldsymbol{H}^{\mathrm{T}}\hat{\Psi}_k^{-1} \end{cases} \tag{7}$$

3.2 Parameter estimation by the ML

In (6) and (7), except for the constant parameters $\gamma_1, \gamma_2, \ldots, \gamma_{2M-1}, \gamma_{2M}, \varepsilon$, the initial state $\boldsymbol{X}_{0|0}$ and the initial conditional variance $\boldsymbol{S}_{0|0} = \mathrm{diag}([s_1\, s_2 \ldots s_{2M-1}\, s_{2M}])$ also need to be estimated. So the parameters to be estimated are $\boldsymbol{\theta} = (\gamma_1, \ldots, \gamma_{2M}, \varepsilon, x_{1,0}, \ldots, x_{2M,0}, s_1, \ldots, s_{2M})$. Assuming $\boldsymbol{v}_k$ is a Gaussian white noise vector with covariance Ψ_k, then the joint conditional density of $\boldsymbol{v}_k$ may be written as

$$p(\boldsymbol{v}_k | y_{k-1}, \ldots, y_1, \boldsymbol{\theta}) = \frac{1}{2\pi|\Psi_k|^{1/2}}\exp\left(-\frac{1}{2}v_k^{\mathrm{T}}\Psi_k^{-1}\boldsymbol{v}_k\right) \tag{8}$$

where $|\bullet|$ denotes the determinant. Therefore, (−2) log-likelihood of the model (3) may be derived as follows:

$$\begin{aligned} &(-2)\log p(y_N, \ldots, y_1 | \boldsymbol{\theta}) \\ &= \sum_{k=1}^{N}(-2)\log p(y_k | y_{k-1}, \ldots, y_1, \boldsymbol{\theta}) \\ &= \sum_{k=1}^{N}(-2)\log p(v_k | y_{k-1}, \ldots, y_1, \boldsymbol{\theta}) \\ &= \sum_{k=1}^{N}\left\{\log|\Psi_k| + v_k^{\mathrm{T}}\Psi_k^{-1}\boldsymbol{v}_k\right\} + N\log 2\pi \end{aligned} \tag{9}$$

where N represents the sampling length.

From the estimated innovation $\hat{v}_k$ and its covariance $\hat{\Psi}_k$ with respect to the given parameters $\boldsymbol{\theta}$, the optimal parameters $\boldsymbol{\theta}^*$ may be obtained by minimising the (−2) log-likelihood function (9) as follows:

$$\begin{aligned} \boldsymbol{\theta}^* = \arg\min_{\boldsymbol{\theta}} &\sum_{k=1}^{N}\left\{\log\left|\hat{\Psi}_k(\boldsymbol{\theta})\right| + (\hat{v}_k(\boldsymbol{\theta}))^{\mathrm{T}}\left(\hat{\Psi}_k(\boldsymbol{\theta})\right)^{-1}(\hat{v}_k(\boldsymbol{\theta}))\right\} \\ &+ N\log 2\pi \end{aligned} \tag{10}$$

In this paper, the function 'FMINSEARCH' based on the Nelder–Mead method in the MATLAB Optimisation Toolbox is used to carry out the parameter optimisation.

4 Simulations

In this section, two kinds of transient travelling wave signals are given to verify the effectiveness of the proposed algorithm. One is simulated by the model (1), and the other is generated by a diversity of fault conditions such as different fault locations, different fault resistances and different fault inception angles using ATP software. Also, the WT is used to detect the travelling wave head for comparison.

4.1 Detection of the transient travelling wave signal simulated by model (1)

The mutation characteristic of the transient travelling wave signal is very similar to the sudden change of the instantaneous pulse, so the travelling wave head can be simulated by a pulse. For simplicity, we assume that the transient travelling wave signal in the model (1) is composed of a fundamental component, travelling wave head and white noise, not harmonic components. Thus, this kind of transient travelling wave signal is considered as follows: (see (11)) . Here, the fundamental frequency f is assumed 50 Hz, constant phase φ and sampling time T_s are 0 rad ($\varphi = 0$ rad) and 100 µs ($T_s = 100\,\mu$s), respectively. Travelling wave head u_t is simulated by $5e^{-5t}$. v_t represents a Gaussian white noise with signal-to-noise ratio (SNR) values of 40, 30, and 20 dB, which means the Gaussian white noise has 0.01, 0.0316 and 0.1 p.u. standard deviation, respectively. Obviously, the time when travelling wave head occurs is from 0.0840 to 0.0845 s, which is very short.

Fig. 1 shows the observed transient travelling wave signals with changes in noise and the clean transient travelling wave signal without noise. Fig. 2 shows comparisons of the estimated signals and amplitudes versus the actual signals and amplitudes between the conventional EKF and the proposed EKF-ML under different noise level conditions. In order to show more subtle differences, the parts of the abrupt changes (the instantaneous pulse) in Fig. 2 are locally magnified. The estimated parameter ε by the EKF-ML is given in Table 1.

In Fig. 2, the estimated signals by the EKF-ML can track the actual signals accurately except that there are small deviations of the estimated value from the actual value in the case of 20 dB SNR. Compared with the EKF, the EKF-ML has better tracking performance and shorter rise time especially on the rising edge of the instantaneous pulse in the locally magnified parts of Fig. 2 (the upper). As shown in Fig. 2, the proposed EKF-ML algorithm can accurately capture the pulse, and the estimated amplitudes roughly match the actual amplitudes in all conditions. Obviously, in the locally magnified parts of Fig. 2 (the lower) where a pulse occurs at different noise levels, the EKF-ML algorithm can quickly and accurately track the rising edge, although the estimated peak is higher than the actual peak in the condition of 20 dB SNR. The response speed of the EKF-ML is quicker than that of the EKF

$$y_t = \begin{cases} \cos(2\pi f t + \varphi) + v_t & 0\,\mathrm{s} \le t < 0.0840\,\mathrm{s} \text{ and } 0.0845\,\mathrm{s} < t \le 0.15\,\mathrm{s} \\ \cos(2\pi f t + \varphi) + 5e^{-5t} + v_t & 0.0840\,\mathrm{s} \le t \le 0.0845\,\mathrm{s} \end{cases} \tag{11}$$

© The Institution of Engineering and Technology 2017

when they track the rising edge of the instantaneous pulse. The fast response to the instantaneous pulse can provide more precise fault location based on the quick and effective wave head detection. In Table 1, it can be seen that the values of the estimated parameter ε by the EKF-ML are very close to the actual values in all conditions, while the conventional EKF needs a given noise parameter value. Thus, the accurate estimation of the observation noise covariance matrix can further ensure that the EKF has better accuracy and faster convergence. This also verifies the effectiveness and the accuracy of the proposed algorithm.

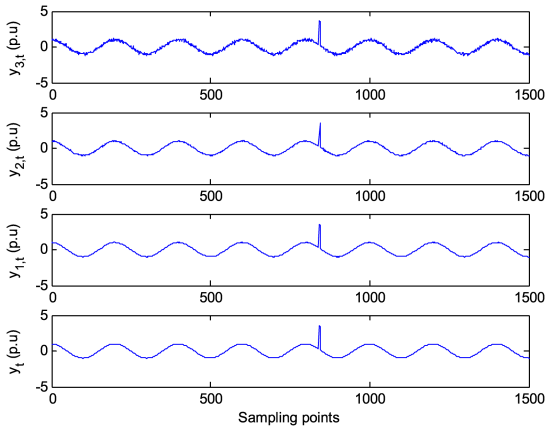

Fig. 1 *Observed sinusoidal signals and the clean sinusoidal signal (y_t, $y_{1,t}$, $y_{2,t}$, $y_{3,t}$ denote the clean signal without noise and the observed signals disturbed with SNR values of 40, 30, and 20 dB, respectively)*

4.2 Fault location based on the detection of the travelling wave head

In order to explore the effectiveness of the detection of the travelling wave head, fault location is performed through the EKF-ML based on the double-ended travelling wave method. The transient current signals from single phase-to-ground faults are simulated at different fault conditions such as different fault locations, different fault resistances and different fault inception angles using the ATP software. The data is captured by travelling wave recorders at substations M and N on a 220 kV power grid. The sampling rate is 5 MHz in this simulation, and L ($L = 150$ km) is the total length of the fault transmission line from substation M to substation N. According to the double-ended method [15], the fault distance d_1 from the fault point to the substation M can be computed as

$$d_1 = \frac{L + v(t_1 - t_2)}{2} \tag{12}$$

Here, v is the travelling wave velocity, which may be taken as 2.96912×10^8 m/s. t_1 and t_2 represent the time when a fault travelling wave arrives at the substations M and N, respectively. Obviously, only if the time t_1 and t_2 are determined, it is easy to calculate the fault distance.

The effectiveness of the proposed fault location method is evaluated using the absolute error Δd and the relative error $\Delta d\%$ which are calculated as follows:

$$\Delta d = |d - d_1|, \quad \Delta d\% = \frac{|d - d_1|}{L} \times 100\% \tag{13}$$

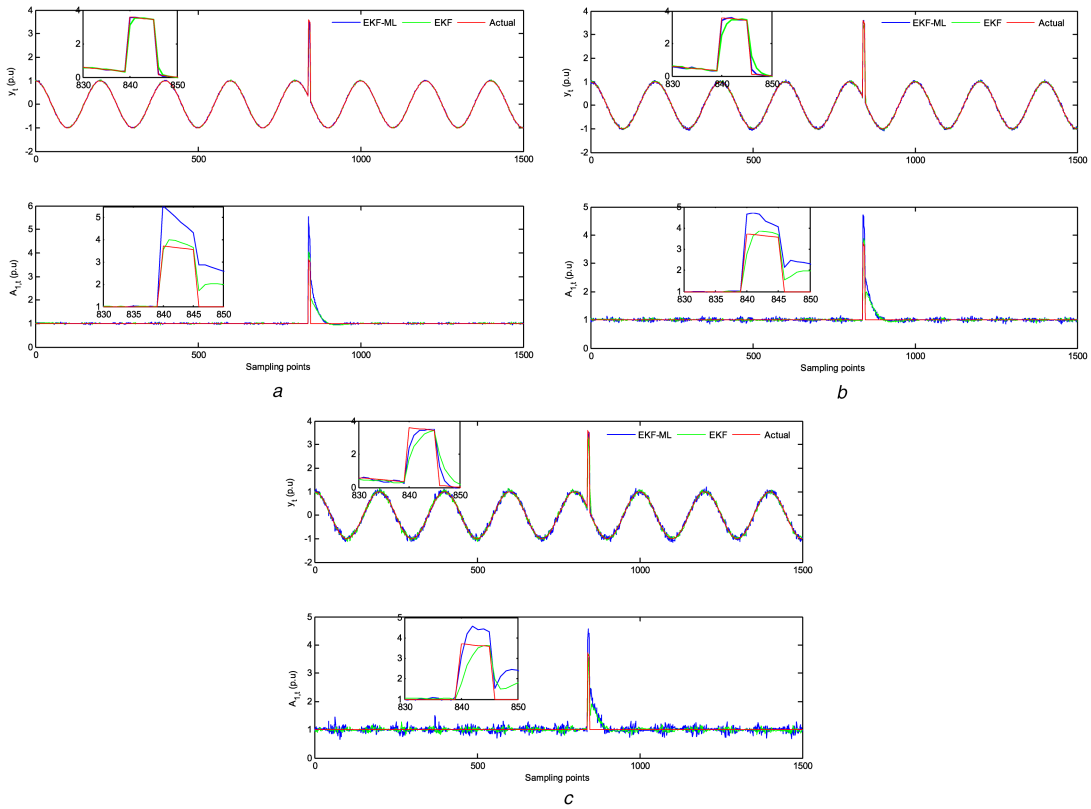

Fig. 2 *Estimated signal and amplitude using the EKF-ML and the EKF at different noise levels*
(a) SNR = 40 dB, ***(b)*** SNR = 30 dB, ***(c)*** SNR = 20 dB

Table 1 Estimated parameter ε by the EKF-ML

Noise, dB	Estimation	Actual
40	0.00970	0.0100
30	0.0297	0.0316
20	0.101	0.100

© The Institution of Engineering and Technology 2017

where d, d_1, L denote the actual fault distance, the calculated fault distance and the total length of the transmission line, respectively.

4.2.1 Case 1: The effect of different fault locations: In this part, different fault locations are simulated to verify the accuracy of the method. In this simulation, the fault resistance value selected is 200 Ω and the fault inception angle is 80°. Also, Gaussian white noise is added to the travelling signal with the SNR of 20 dB. The fault distance parameter d is set to 20, 45, 50, 60, 75, 90, 105, 120 and 135 km. Fig. 3 gives the travelling current signals interfered by the Gaussian white noise of 20 dB with different fault locations from the substations M (red) and N (blue). Fig. 4 shows the estimated amplitudes of the travelling wave signals from the substations M and N. The fault location results for different fault locations are shown in Table 2.

In Fig 4, it is clear that the instantaneous amplitudes change dramatically when the head of travelling wave arrives, and the sharp singularity points can be easily detected, which are marked. Therefore, the travelling wave head arriving time is computed and the fault distance can be calculated using relation (12) from the first singularity points at the substations M and N. From Table 2, it is clear that the accuracy of the proposed method is significantly good for determining fault distance at different fault locations. The maximum absolute error and relative error are 0.320 km and 0.213%, respectively, at fault distance of 135 km from the substation M, while the minimum absolute error and relative error are 0. Hence, the nearer the fault point is to the mid-point of the line, the higher the fault location accuracy is. Instead, as the fault point is near to the substation (M or N), the fault location error

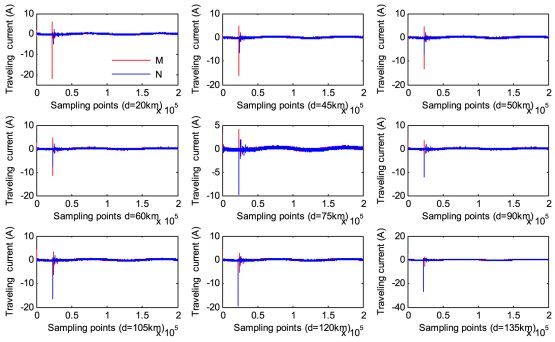

Fig. 3 *Travelling current signals interfered by white noise with different fault locations (red: M, blue: N)*

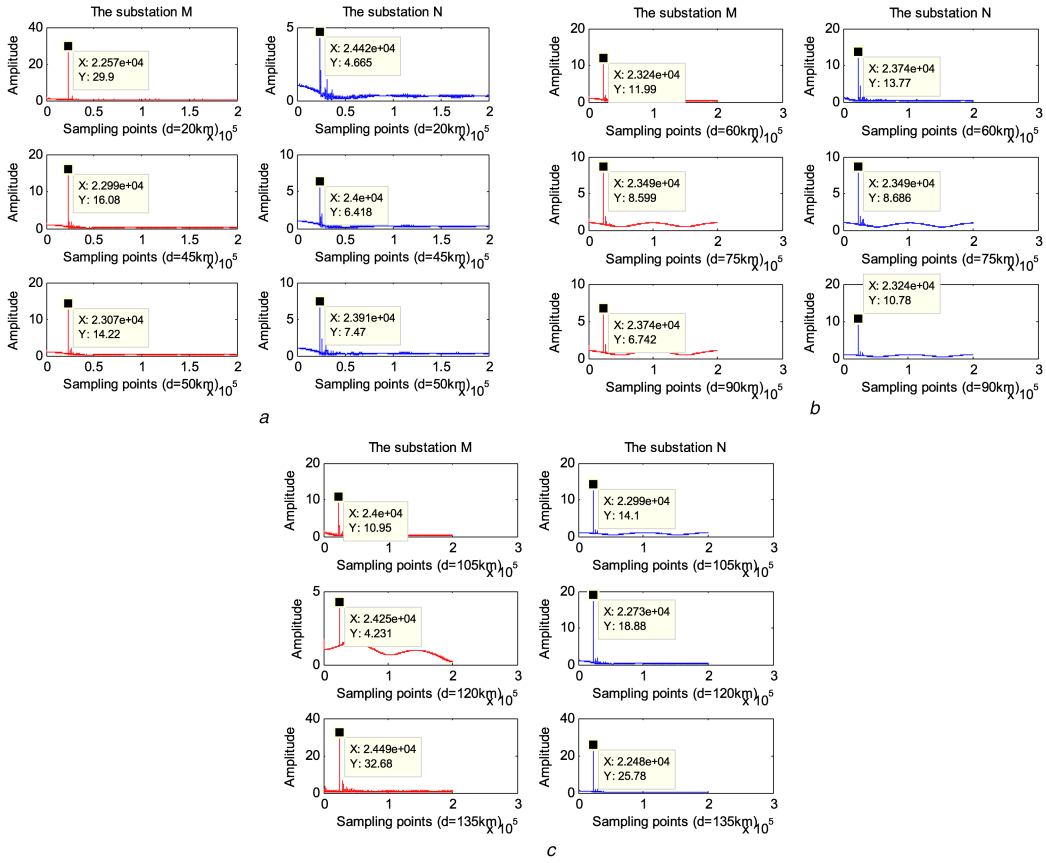

Fig. 4 *Estimated amplitudes of the travelling wave signals from the substations M (red) and N (blue)*
(a) $d = 20, 45, 50$ km, ***(b)*** $d = 60, 75, 90$ km, ***(c)*** $d = 105, 120, 135$ km

Table 2 Obtained result of different fault locations using the EKF-ML

d, km	M	N	d_1, km	Δd, km	Δd, %
20	22,570	24,420	20.071	0.071	0.0473
45	22,990	24,000	45.011	0.011	0.00733
50	23,070	23,910	50.059	0.059	0.0393
60	23,240	23,740	60.154	0.154	0.103
75	23,490	23,490	75	0	0
90	23,740	23,240	89.846	0.154	0.103
105	24,000	22,990	104.988	0.012	0.008
120	24,250	22,730	120.130	0.130	0.0867
135	24,490	22,480	134.680	0.320	0.213

© The Institution of Engineering and Technology 2017

becomes increasing. Maybe this is because any detecting method has delay time when it extracts the singularity points, thus, the EKF-ML has almost the same response time for the detecting the singularity points at the substations M and N when the fault point is close to the mid-point of the transmission line (the distance between the fault point and the substation M is as well as that at the fault point and the substation N). Moreover, with the increase of the propagation distance, the high components of the transient travelling wave have larger attenuation. Thus, the time difference of the initial wave front arriving at both substations becomes large when the fault point is close to the substation, so the fault location error becomes increasing.

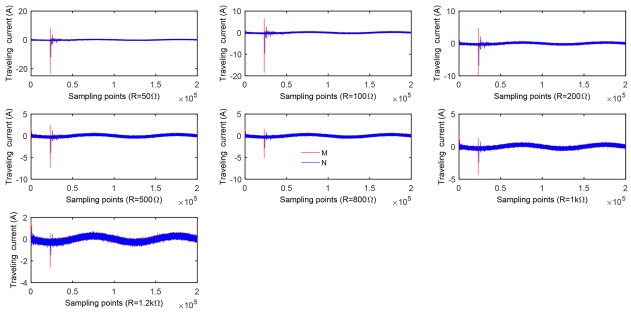

Fig. 5 *Travelling current signals interfered by white noise with different fault resistances (red: M, blue: N)*

4.2.2 Case 2: The effect of different fault resistances: In this simulation, the fault resistance is varying from 50 to 1200 Ω, and the fault inception angle is 80°and the fault distance is set a fixed value, namely $d = 50$ km. Also, Gaussian white noise is added to the travelling signal with the SNR of 20 dB. Fig. 5 gives the travelling current signals interfered by the Gaussian white noise of 20 dB with different fault resistances at the substations M (red) and N (blue). Fig. 6 shows the estimated amplitudes of the travelling wave signals from the substations M and N, and the sharp singularity points are marked in Fig. 6. Table 3 gives the fault location results with varying fault resistances.

From Table 3, it can be seen that the calculated fault distances (d_1) are all 50.059 km, which are very close to the actual fault distance (50 km). This indicates that the accuracy of the fault location is not affected by the fault resistance. The detected singularity points at the substations M and N are 23,070 and 23,910, respectively, as the fault resistance is varying from 50 to 500 Ω. With increasing fault resistance from 800 to 1200 Ω, the

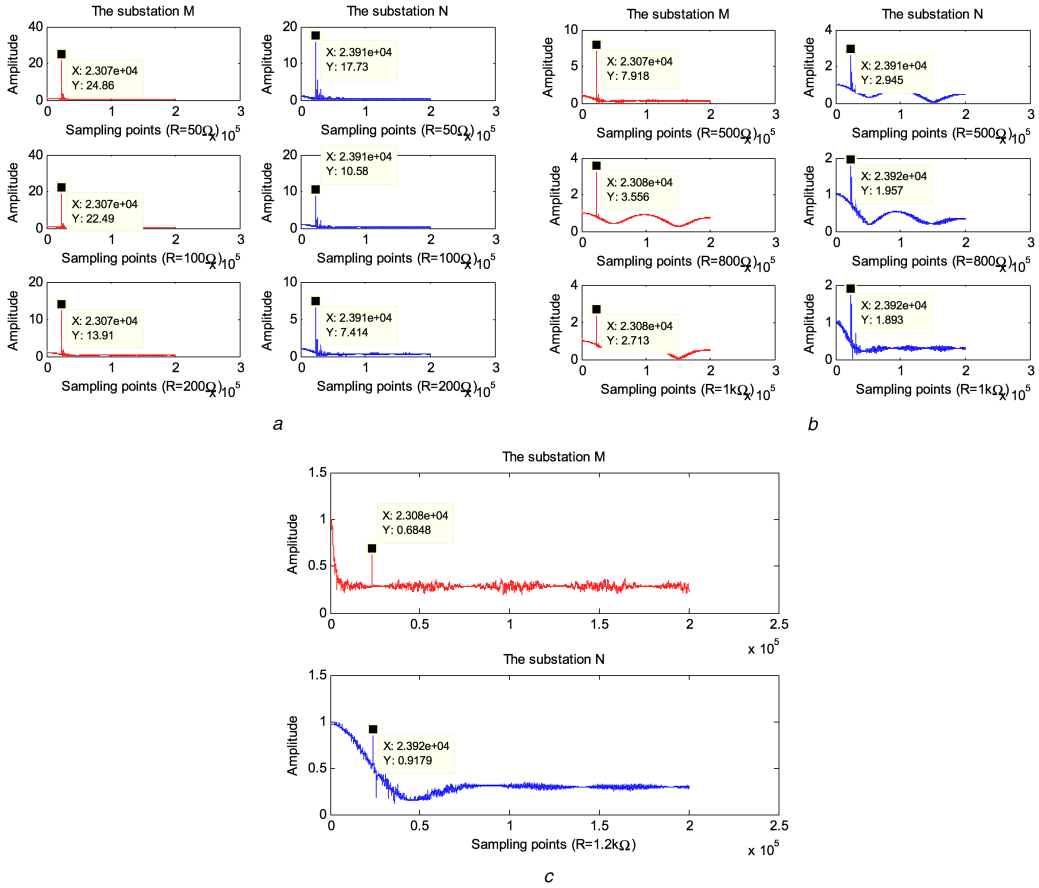

Fig. 6 *Estimated amplitudes of the travelling wave signals from the substations M (red) and N (blue)*
(a) $R = 50, 100, 200$ Ω, ***(b)*** $R = 500, 800, 1000$ Ω, ***(c)*** $R = 1200$ Ω

Table 3 Obtained result of different fault resistances using the EKF-ML

R, Ω	M	N	d_1, km	Δd, km	Δd, %
50	23,070	23,910	50.059	0.059	0.0393
100	23,070	23,910	50.059	0.059	0.0393
200	23,070	23,910	50.059	0.059	0.0393
500	23,070	23,910	50.059	0.059	0.0393
800	23,080	23,920	50.059	0.059	0.0393
1000	23,080	23,920	50.059	0.059	0.0393
1200	23,080	23,920	50.059	0.059	0.0393

© The Institution of Engineering and Technology 2017

detected singularity points at the substations M and N are changed to 23,080 and 23,920, respectively. By comparison, the latter has 10 sampling points delay, but the time delay is identical between the substations M and N. Thus, the arriving time difference of the wave head between the substations M and N remains unchanged. From Fig. 5, we can see that travelling signals become weak with increasing fault resistances. This result is in agreeing with that shown in Fig. 6 where the estimated amplitudes become decreasing with increasing fault resistances.

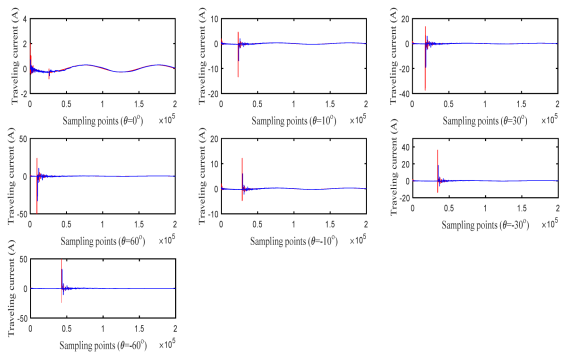

Fig. 7 *Travelling current signals interfered by white noise with different fault inception angles (red: M, blue: N)*

4.2.3 Case 3: The effect of different fault inception angles: To consider the effect of fault inception angle on the performance of the proposed method, the proposed method is tested for a wide range of fault inception angle from −60° to 60°. The fault resistance is 800 Ω and the fault distance is set a fixed value, namely $d = 50$ km. Also, Gaussian white noise is added to the travelling signal with the SNR of 20 dB. Fig. 7 gives the travelling current signals interfered by the Gaussian white noise of 20 dB with different fault inception angles at the substations M (red) and N (blue). Fig. 8 shows the estimated amplitudes of the travelling wave signals from the substations M and N, and the sharp singularity points are marked in Fig. 8. Table 4 gives the fault location results with varying fault inception angles.

In Fig. 7, it is easy to see that the travelling signal at 0° fault inception angle gets the weakest. In Fig. 8, the detected singularity points at the substations M and N are changing with changing fault inception angles, but singularity point difference between the substations M and N is unchanged except in case of 0° fault inception angle, i.e. the arriving time difference of the wave head between the substations M and N remains unchanged. As shown in Table 4, the calculated fault distances (d_1) are all 50.059 km except

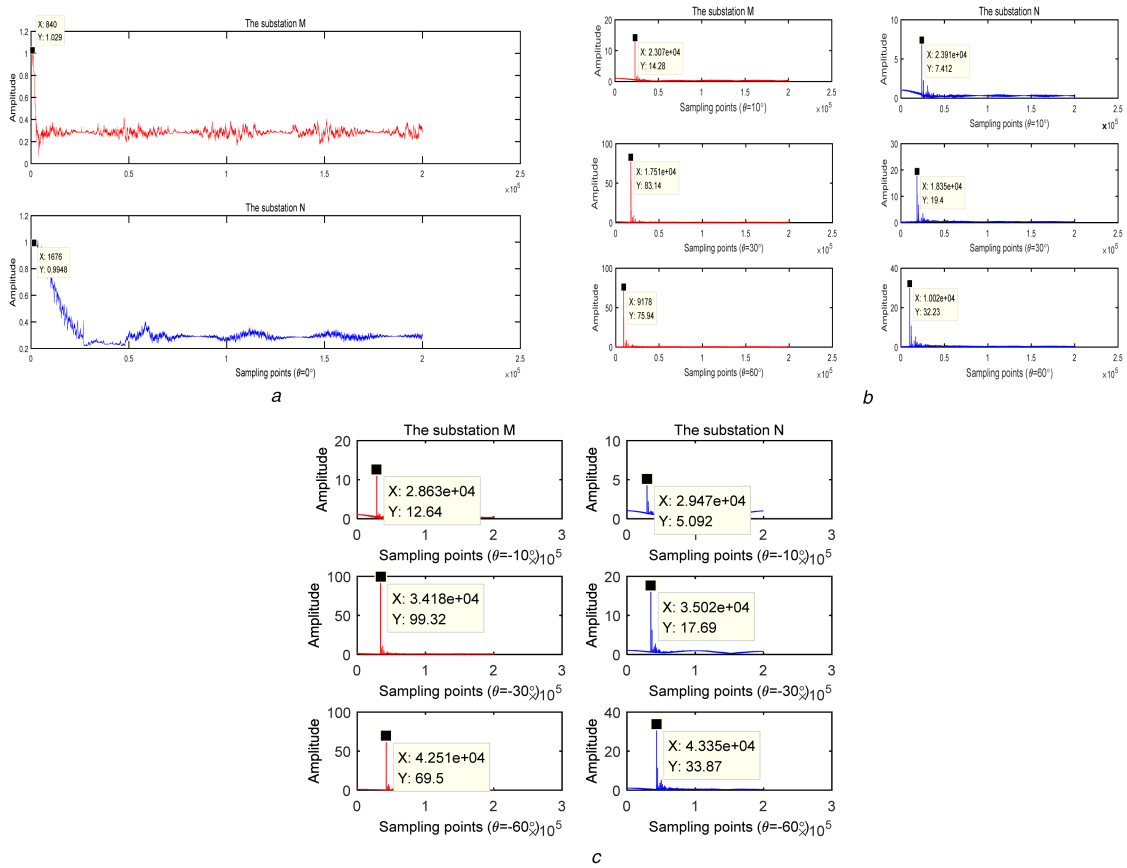

Fig. 8 *Estimated amplitudes of the travelling wave signals from the substations M (red) and N (blue)*
(a) $\theta = 0°$, ***(b)*** $\theta = 10°, 30°, 60°$, ***(c)*** $\theta = -10°, -30°, -60°$

Table 4 Obtained result of different fault inception angles using the EKF-ML

θ	M	N	d_1, km	Δd, km	Δd, %
0°	840	1676	50.178	0.178	0.119
10°	23,070	23,910	50.059	0.059	0.0393
30°	17,510	18,350	50.059	0.059	0. 0393
60°	9178	10,020	50.059	0.059	0.0393
−10°	28,630	29,470	50.059	0.059	0.0393
−30°	34,180	35,020	50.059	0.059	0.0393
−60°	42,510	43,350	50.059	0.059	0.0393

© The Institution of Engineering and Technology 2017

Table 5 Obtained result of different fault locations using the WT

d, km	M	N	d_1, km	Δd, km	Δd, %
20	22,560	24,420	19.774	0.226	0.151
45	22,980	23,980	45.309	0.309	0.206
50	23,080	23,910	50.356	0.356	0.237
60	23,230	23,730	60.154	0.154	0.103
75	23,490	23,490	75	0	0
90	23,730	23,230	89.846	0.154	0.103
105	23,980	22,980	104.691	0.309	0.206
120	24,220	22,730	119.240	0.760	0.507
135	24,480	22,480	134.382	0.618	0.412

Table 6 Obtained result of different fault resistances using the WT

R, Ω	M	N	d_1, km	Δd, km	Δd, %
50	23,080	23,910	50.356	0.356	0.0393
100	23,080	23,910	50.356	0.356	0.0393
200	23,080	23,910	50.356	0.356	0.0393
500	23,080	23,910	50.356	0.356	0.0393
800	23,080	23,910	50.356	0.356	0.0393
1000	23,080	23,910	50.356	0.356	0.0393
1200	23,080	23,940	49.466	0.534	0.356

Table 7 Obtained result of different fault inception angels using the WT

θ	M	N	d_1, km	Δd, km	Δd, %
0°	848	1680	50.297	0.297	0.198
10°	23,080	23,910	50.356	0.356	0.237
30°	17,510	18,350	50.059	0.059	0.0393
60°	9183	10,010	50.445	0.445	0.297
−10°	28,610	29,440	50.356	0.356	0.237
−30°	34,170	34,990	50.653	0.653	0.435
−60°	42,500	43,330	50.356	0.356	0.23%

in case of 0° fault inception angle, which is very close to the actual fault distance (50 km). Obviously, when the travelling signal get the weakest (at 0° fault inception angle), the absolute error and relative error reach the maximum (0.178 and 0.119%). Moreover, the detected singularity points at 0° fault inception angle are not so clear as those at the other fault inception angles. However, the absolute error at 0° fault inception angle is <500 m, and the accuracy of fault location is still high. This demonstrates that the proposed method is effective in distinguishing weak travelling signals.

To verify the superiority of the proposed algorithm, the WT is applied for travelling wave-based fault location for comparison. In this simulation, Daubechies discrete wavelet of order 4 (db4) is used to distinguish the above travelling wave signals under different fault conditions because Daubechies wavelets are the family of orthogonal wavelets and the db4 exhibits more efficient in feature extraction. First, the travelling wave signal is denoised by wavelet threshold to remove random noise from the original travelling wave signal. After denoising, the signal can be reconstructed using inverse discrete WT. Then, four layer Daubechies wavelet decomposition is applied to the signal that has been denoised. Tables 5–7 give the fault location results.

Obviously, when travelling wave signals get weak, the sharp singularity points are submerged in the noise and could hardly be clearly detected by the WT especially under these conditions of 1200 Ω fault resistance and 0° fault inception angle. Hence, the performance of the WT deteriorates in case of weak travelling signals. By comparisons between Tables 2–4 and 5–7, the accuracy of fault location by the EKF-ML is remarkably higher than that by the WT except for some cases.

Moreover, the fault location results show that the EKF-ML has better robustness than does the WT, especially for different fault inception angles. On the other hand, the two methods have the minimum error and perform the best when the fault point is close to the mid-point of the transmission line.

5 Conclusions

In this paper, a new adaptive method is proposed for analysing the initial travelling waves and for online locating faults. In this method, first, the EKF algorithm based on ML method is used to estimate the optimal states (the clean travelling waves) with additive white noise. Then, the amplitudes of the travelling waves are calculated by the estimated states and the sharp singularity points of the amplitudes are detected. The effectiveness of exacting mutation feature using the proposed method has been demonstrated by the travelling wave in the model (1), which is simulated by an instantaneous pulse. Further, the performance of the proposed method is tested with various fault scenarios including different fault locations, different fault resistances, and different fault inception angles. The results show that the method has high accuracy and noise immunity even though the travelling wave is weak because of high fault resistances or single phase faults with inception angle close to 0°, or the fault location is very near the substation ends. Besides, the proposed method is robust and insensitive to fault resistance and phase angle. When compared with other travelling wave-based methods, such as the WT, fault location can be estimated more accurately using the EKF-ML especially for the weak travelling waves.

6 Acknowledgments

This work was supported by the National Science Foundation of China (51507015, 61540037, 71271215, 61233008, 51425701, 70921001, 51577014, 51507014), and the Natural Science Foundation of Hunan Province (2015JJ3008), and the National key research and development program of China (2016YF0900605).

© The Institution of Engineering and Technology 2017

7 References

[1] Xu, W., Jing, Y.: 'Power disturbance data analytics – new application of power quality monitoring data'. Proc. Chinese Society for Electrical Engineering (CSEE), Chengdu, China, 2013, pp. 93–101

[2] Saha, M.M., Izykowski, J., Rosolowski, E.: '*Fault location on power networks*' (Springer Science & Business Media, 2009)

[3] Zhang, G., Shu, H., Liao, Y.: 'Automated double-ended traveling wave record correlation for transmission line disturbance analysis', *Electr. Power Syst. Res.*, 2016, **136**, pp. 242–250

[4] Wang, W., Zeng, X., Yan, L., *et al.*: 'Principle and control design of active ground-fault arc suppression device for full compensation of ground current', *IEEE Trans. Ind. Electron.*, 2017, **64**, pp. 4561–4570

[5] García-Gracia, M., Montañés, A., El Halabi, N., *et al.*: 'High resistive zero-crossing instant faults detection and location scheme based on wavelet analysis', *Electr. Power Syst. Res.*, 2012, **92**, pp. 138–144

[6] Livani, H., Evrenosoglu, C.Y.: 'A single-ended fault location method for segmented HVDC transmission line', *Electr. Power Syst. Res.*, 2014, **107**, pp. 190–198

[7] Liang, R., Wang, F., Fu, G., *et al.*: 'A general fault location method in complex power grid based on wide-area traveling wave data acquisition', *Int. J. Electr. Power Energy Syst.*, 2016, **83**, pp. 213–218

[8] Ray, P., Mishra, D.P.: 'Support vector machine based fault classification and location of a long transmission line', *Eng. Sci. Technol. Int. J.*, 2016, **19**, (3), pp. 1368–1380

[9] Yusuff, A.A., Jimoh, A.A., Munda, J.L.: 'Fault location in transmission lines based on stationary wavelet transform, determinant function feature and support vector regression', *Electr. Power Syst. Res.*, 2014, **110**, pp. 73–83

[10] Adewole, A.C., Tzoneva, R., Behardien, S.: 'Distribution network fault section identification and fault location using wavelet entropy and neural networks', *Appl. Soft Comput.*, 2016, **46**, pp. 296–306

[11] Zin, A.A.M., Saini, M., Mustafa, M.W., *et al.*: 'New algorithm for detection and fault classification on parallel transmission line using DWT and BPNN based on Clarke's transformation', *Neurocomputing*, 2015, **168**, pp. 983–993

[12] Yadav, A., Swetapadma, A.: 'A single ended directional fault section identifier and fault locator for double circuit transmission lines using combined wavelet and ANN approach', *Int. J. Electr. Power Energy Syst.*, 2015, **69**, pp. 27–33

[13] Reddy, M.J., Mohanta, D.K.: 'A wavelet-fuzzy combined approach for classification and location of transmission line faults', *Int. J. Electr. Power Energy Syst.*, 2007, **29**, (9), pp. 669–678

[14] Zhang, X.L., Zeng, X.J., Li, Z.W., *et al.*: 'Traveling wave fault location of transmission line using Hilbert-Huang transform'. Third Int. Conf. Electric Utility Deregulation and Restructuring and Power Technologies, Nanjing, China, 2008, pp. 1–6

[15] Bernadić, A., Leonowicz, Z.: 'Fault location in power networks with mixed feeders using the complex space-phasor and Hilbert–Huang transform', *Int. J. Electr. Power Energy Syst.*, 2012, **42**, (1), pp. 208–219

[16] Xu, L.G., Jian, J., Tianye, G., Yongshen, M.: 'Power systems faults location with traveling wave based on Hilbert–Huang transform'. Int. Conf. Energy and Environment Technology, Guilin, China, 2009, pp. 197–200

[17] Li, Z.H.: 'Hilbert–Huang transform based application in power system fault detection'. Int. Workshop on Intelligent Systems and Applications, Wuhan, China, 2009, pp. 1–4

[18] Ali, N.H., Ali, B.M., Basir, O., *et al.*: 'Protection of smart substation based on WLAN complies with IEC 61850 using traveling wave analysis', *Electr. Power Syst. Res.*, 2016, **140**, pp. 20–26

[19] Mostafa, M.A.: 'Kalman filtering algorithm for electric power quality analysis: harmonics and voltage sags problems'. Proc. Large Engineering Systems Conf. Power Engineering, Montreal, Canada, 2007, pp. 159–165

[20] Li, Y., Huang, Z., Zhou, N., *et al.*: 'Application of ensemble Kalman filter in power system state tracking and sensitivity analysis'. IEEE/PES Transmission and Distribution Conf. and Exposition (T&D), Orlando, Florida, USA, 2012, pp. 1–8

[21] Li, C.J., Chen, J.C., Huang, S., *et al.*: 'Research on the wave head detecting algorithm based on Kalman filtering'. 5th Int. Conf. Electric Utility Deregulation and Restructuring and Power Technologies, Changsha, China, 2015, pp. 1074–1079

[22] Hasan, S., Dash, P.K., Panigrahi, B.K., *et al.*: 'Adaptive unscented filtering technique and particle swarm optimization for estimation of non-stationary signal parameters'. Proc. IEEE Conf. Industrial Electronics and Applications, Kuala Lumpur, Malaysia, 2009, pp. 3853–3858

[23] Dash, P.K., Mallick, R.K.: 'Accurate tracking of harmonic signals in VSC-HVDC systems using PSO based unscented transformation', *Int. J. Electr. Power Energy Syst.*, 2011, **33**, (7), pp. 1315–1325

[24] Dash, P.K., Hasan, S., Panigrahi, B.K.: 'A hybrid unscented filtering and particle swarm optimization technique for harmonic analysis of nonstationary signals', *Measurement*, 2010, **43**, (10), pp. 1447–1457

[25] Siavashi, E.M., Rouhani, A., Moslemi, R.: 'Detection of voltage sag using unscented Kalman smoother'. Proc. Int. Conf. Environment and Electrical Engineering (EEEIC), Prague, Czech Republic, 2010, pp. 128–131

[26] Jatoth, R.K., Reddy, G.A.: 'A hybrid GA-adaptive particle swarm optimization based tuning of unscented Kalman filter for harmonic estimation'. Proc. Swarm, Evolutionary, and Memetic Computing, Chennai, India, 2010, pp. 380–388

© The Institution of Engineering and Technology 2017